creative commons
COMMONS DEED

저작자표시-비영리-변경금지 2.0 대한민국

이용자는 아래의 조건을 따르는 경우에 한하여 자유롭게

- 이 저작물을 복제, 배포, 전송, 전시, 공연 및 방송할 수 있습니다.

다음과 같은 조건을 따라야 합니다:

저작자표시. 귀하는 원저작자를 표시하여야 합니다.

비영리. 귀하는 이 저작물을 영리 목적으로 이용할 수 없습니다.

변경금지. 귀하는 이 저작물을 개작, 변형 또는 가공할 수 없습니다.

- 귀하는, 이 저작물의 재이용이나 배포의 경우, 이 저작물에 적용된 이용허락조건을 명확하게 나타내어야 합니다.
- 저작권자로부터 별도의 허가를 받으면 이러한 조건들은 적용되지 않습니다.

저작권법에 따른 이용자의 권리는 위의 내용에 의하여 영향을 받지 않습니다.

이것은 이용허락규약(Legal Code)을 이해하기 쉽게 요약한 것입니다.

Disclaimer

dCollection

공학석사 학위논문

Model Predictive Control for Reducing NO_x Emissions from Diesel Exhaust Aftertreatment System

디젤 배기가스 후처리 시스템의 NO_x 저감을 위한 모델예측제어

2020년 2월

서울대학교 대학원
화학생물공학부
이 병 준

Abstract

Model Predictive Control for Reducing NO_x Emissions from Diesel Exhaust Aftertreatment System

Byungjun Lee
School of Chemical and Biological Engineering
The Graduate School
Seoul National University

This thesis proposes a nonlinear model predictive control scheme which maximizes the $\mathbf{NO}_x$ removal performance of diesel exhaust aftertreatment system using post injection and urea injection control. One-dimensional sequential catalytic converter model, which consists of diesel oxidation catalyst (DOC), diesel particulate filter (DPF), and selective catalytic reduction (SCR), is designed to describe the diesel exhaust aftertreatment system. Also, post injection map, which accounts how rich mode operation changes the concentration and the temperature of engine raw emissions, is also constructed. Using the fact that $\mathbf{NO}_x$ removal performance of SCR is maximized when the $\mathbf{NO_2}/\mathbf{NO}_x$ ratio at the inlet of SCR is 0.5, post injection controller is designed with the combination of $\mathbf{NO}_x$ controller and PM controller. In addition, successive linearization based method is used to reduce the computational cost for real-time implementation of model predictive control. As a result, proposed control

scheme reduces more than half of cumulative $\mathbf{NO}_x$ while minimizing additional fuel consumption compared to the reference case which has no $\mathbf{NO}_x$ controller.

Keywords: Emission control, Model predictive control, Diesel oxidation catalyst (DOC), Diesel Particulate Filter (DPF), Selective Catalytic Reduction (SCR)
Student Number: 2018-23056

Contents

List of Tables

List of Figures

Chapter 1

Introduction

Diesel engines are more fuel-efficient than gasoline engines, but emission standards for diesel vehicles are getting more stringent [1, 2] due to large $\mathbf{NO}_x$ and particulate matter (PM) emissions. $\mathbf{CO}$, hydrocarbon (HC), PM, $\mathbf{SO_2}$, and $\mathbf{NO}_x$ are common air pollutants emitted from diesel engines [3], and these pollutants should be removed by installing additional exhaust aftertreatment devices. PM can cause a lot of serious health problems like asthma, respiratory diseases, cardiovascular diseases, and lung cancer [4]. Furthermore, $\mathbf{CO}$, $\mathbf{NO}_x$, $\mathbf{SO_2}$ are indirect green house gases that facilitate greenhouse gas production through chemical reactions [3].

$\mathbf{CO}$ and HC are removed from diesel oxidation catalyst (DOC), by oxidation reaction with $\mathbf{O_2}$ [5]. Also, PM is removed from diesel particulate filter (DPF), by filtering and regeneration. DPF regeneration is usually done by oxidation with $\mathbf{NO_2}$ in the temperature range of 250°C $\sim$ 400°C, and this process is called passive regeneration [6]. However, the pressure drop through the DPF filter increases as the PM accumulates in DPF due to the slow process of passive regeneration. In this case, active regeneration by $\mathbf{O_2}$ should be processed at a temperature above 550°C [6], and this range of temperature can be achieved by additional fuel injection [3]. In addition, $\mathbf{NO}_x$ is con-

verted to $\mathbf{N_2}$ by selective catalytic reduction (SCR) where $\mathbf{NH_3}$ degraded from urea solution acts as a reducing agent [7]. Since DOC is a key device that enables DPF to reach a temperature above 550°C for active regeneration by oxidation reactions from additional fuel injection [8], conventional order of diesel exhaust aftertreatment system is DOC-DPF-SCR. The overview of diesel exhaust aftertreatment system is introduced in figure 1.1.

The most challenging technique required for diesel vehicles is SCR, because of tight $\mathbf{NO}_x$ emissions standards by Euro6 which were applied to all new cars beginning on September, 2015. It requires to reduce $\mathbf{NO}_x$ emissions level to 80mg/km based on the laboratory test, and this level is 55.6% less than Euro5 emission standards as it is shown in figure 1.2. Furthermore, Euro6-TEMP regulation is applied beginning on September, 2017, which includes the real driving emissions (RDE) test. It requires to reduce $\mathbf{NO}_x$ emissions level to 168mg/km based on the RDE test, and it will be more tightend to 120mg/km when Euro6d regulation starts from 2021 [1].

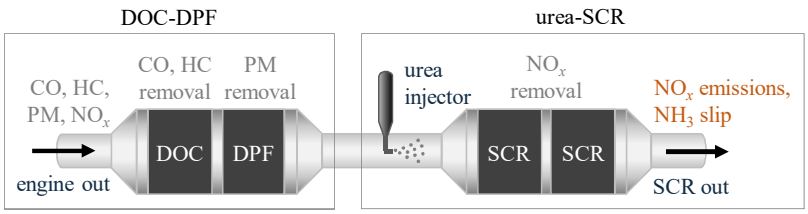

Figure 1.1: Overview of diesel exhaust aftertreatment system

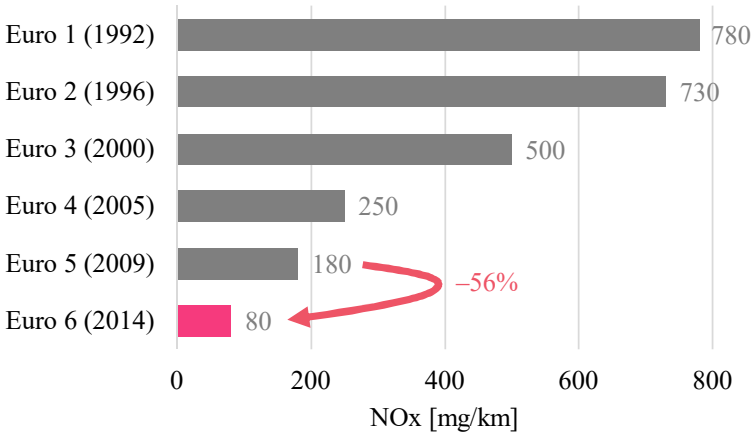

Figure 1.2: $\mathbf{NO}_x$ emission standards for passenger cars

There are two actuators we can control to reduce the $\mathbf{NO}_x$ emissions level. First one is an urea injector, which injects an aqueous urea solution into the SCR to supply $\mathbf{NH_3}$ by degradation reactions. In this case, urea injection rate is a manipulated variable. If urea injection rate increases, more $\mathbf{NH_3}$ adsorbs to the active site of SCR, and it increases SCR coverage ratio. The increase of SCR coverage ratio leads to a decrease of $\mathbf{NO}_x$ emissions, while $\mathbf{NH_3}$ slip increases and fuel efficiency decreases. To optimize a trade-off between $\mathbf{NO}_x$ emissions and $\mathbf{NH_3}$ slip while maximizing the fuel efficiency, we have to control the SCR coverage ratio through the urea injector rate. For this reason, a mathematical model of SCR is required which accounts its geometric information, mass and energy balancess, and chemical reactions. There are three types of SCR reactions between adsorbed $\mathbf{NH_3}$ and $\mathbf{NO}_x$, and the reaction which $\mathbf{NH_3}$ reacts with equimolar $\mathbf{NO - NO_2}$ is the fastest among the three [2]. Intuitively, we can expect that the $\mathbf{NO}_x$ reduction performance of SCR would be maximized if $\mathbf{NO_2}/\mathbf{NO}_x$ ratio at the SCR inlet reaches $\mathbf{0.5}$, and it was actually proved by the experiment with metal-exchanged zeolites that are used as SCR catalysts [9, 10].

The second actuator is a post injection, which is a delayed fuel injection after a main injection in order to elevate the DPF inlet temperature for active regeneration through the oxidation reactions in DOC. It affects the $\mathbf{NO_2}/\mathbf{NO}_x$ ratio at the SCR inlet because it is sensitive to the temperature due to the equilibrium reaction between $\mathbf{NO}$ and $\mathbf{NO_2}$ [11, 12]. Since the temperature difference between passive and active regeneration in DPF is in the range of 150°C $\sim$ 300°C, we cannot ignore the temperature effect of $\mathbf{NO - NO_2}$ equilibrium on the $\mathbf{NO_2}/\mathbf{NO}_x$ ratio. Furthermore, passive regeneration,

CO and HC oxidation with $\mathbf{NO_2}$, and $\mathbf{NO}$ formation reactions in DPF change the molar amount of $\mathbf{NO}$ and $\mathbf{NO_2}$ which leads to the change of $\mathbf{NO_2}/\mathbf{NO}_x$ ratio [13]. In order to account for the relationship between the post injection and the $\mathbf{NO_2}/\mathbf{NO}_x$ ratio at the SCR inlet, mathematical models of diesel engine, DOC, and DPF are required.

However, the relationship between the post injection and engine raw emissions is quite complex, because complicated combination of mechanical and chemical balance equations affect the concentration and the temperature of engine raw emissions. We can simplify this problem by creating a 'post injection map' that accounts the relationship between the post injection and engine raw emissions for off-line calculation. This idea was initially introduced in the paper of Kim (2018) [14], which is about the control of a sequential catalytic converter consists of lean $\mathbf{NO}_x$ trap (LNT) and urealess SCR (passive SCR, pSCR). However, it did not considered DOC-DPF system in front of the LNT-pSCR system, therefore the application range of post injection map will be broadened to the whole diesel exhaust aftertreatment system (DOC-DPF-SCR) in this thesis. We can further simplify it by fixing the fuel amount per injection and the interval between injections during post injection. In this case, manipulated variable is just a post injection timing, which can be expressed by binary variables; 0 when it is in a lean mode (post injection is not implemented), and 1 when it is in a rich mode (post injection is implemented). However, it is not that simple because the concentration and the temperature of engine raw emissions are sensitive to the consecutive times lean or rich mode was implemented. In other words, it is a function of a sequence of post injection modes.

Model predictive control is therefore an appropriate control algorithm to consider a sequence of post injection modes as a manipulated variable. It compares the several future sequences of post injection modes that were created from each past sequence of post injection modes, and then it selects only the first future input of the optimal future sequence. Model predictive control usually shows excellent tracking performances for constrained nonlinear systems where its stabilities are ensured. However, there is a problem with applying model predictive control to the diesel exhaust aftertreatment system. The computational time to calculate the optimal input often exceeds the sampling time 1s, therefore it is hard to deal with the real driving emissions test. According to Kim (2018) [14], hybrid model predictive control was used due to the highly nonlinear properties of LNT-pSCR and discrete properties of post injection modes, and successive linearization based method was applied to reduce the computational load. In this thesis, application of a successive linearization based model predictive control will be expanded to the whole diesel exhaust aftertreatment system (DOC-DPF-SCR), to propose a solution to the tightening emission standards including real driving emissions test.

Chapter 2 explains about the modeling results to describe the diesel exhaust aftertreatment system and theoretical backgrounds to understand control algorithms which are proposed in chapter 3. Then, chapter 3 proposes two control algorithms and shows the simulation results that compare the $\mathbf{NO}_x$ reduction performances, amounts of cumulative $\mathbf{NH_3}$ slip, and fuel efficiencies of proposed two algorithms.

Chapter 2

Preliminaries

2.1 Post injection map

Post injection is an immediate fuel injection after a relatively longer main injection of diesel engines. This technique is usually targeted to meet the PM regulations of emission standards of diesel engines [15]. Post injection increases the $\mathbf{CO}$ and $\mathbf{HC}$ concentrations and the temperature of engine raw emissions, and then it leads to the increase of oxidation reaction rates in DOC, which results the elevation of DPF inlet temperature. Therefore, it is necessary for DPF to reach the high enough temperature for active regeneration. Without the combination of post injection and DOC, PM accumulates in DPF by the slow process of passive regeneration, which results the high pressure drop through the DPF filter and reduced de$\mathbf{NO}_x$ performance of SCR.

Due to discrete and nonlinear properties of constraints and a complex mechanical structure of diesel engines, manipulated variables for post injection are simplified to binary variables. We define 0 as a lean mode when post injection is not implemented, and 1 as a rich mode when post injection is implemented. Since the concentration and the temperature of engine-out raw emissions are a func-

tion of a sequence of post injection modes, 'post injection map' created by Kim (2018) [14] was used to consider realistic post injection constraints and to reduce the computational load for off-line calculation. When a post injection is implemented, the concentration of $\mathbf{C_3H_6}$, $\mathbf{CO}$, $\mathbf{H_2}$ and the temperature increase while the concentration of $\mathbf{O_2}$ decreases. Its mathematical relationships with a sequence of post injection modes were fitted by averaging 14 different experimental cases.

The example of applying post injection map is shown in figure 2.1 [14]. It considers a sequence of post injection modes during the last 11s including the current time, and there are 175 possible combinations when the constraints of post injection are considered. For each possible previous sequence of post injection modes during the front horizon of length 11, possible sequences of post injection modes during the next 4s are created. Since the delay time of post injection is 1s, post injection mode at a time i and its previous post injection modes determine the states of engine raw emissions at the time $i+\mathbf{1}$ ($u_{i+\mathbf{1}}$), then we can calculate the state changes of engine raw emissions at the time $i+\mathbf{1}$ ($\boldsymbol{\Delta} u_{i+\mathbf{1}} = u_{i+\mathbf{1}} - u_i$).

Previous case	Modes during $t-10 \sim t$										
	$t-10$	$t-9$	$t-8$	$t-7$	$t-6$	$t-5$	$t-4$	$t-3$	$t-2$	$t-1$	t
1	1	1	1	1	1	1	1	1	1	1	0
2	1	1	1	1	1	1	1	1	1	0	0
3	1	1	1	1	1	1	1	1	0	0	1
4	1	1	1	1	1	1	1	1	0	0	0
5	1	1	1	1	1	1	1	0	0	1	1
6	1	1	1	1	1	1	1	0	0	0	1
7	1	1	1	1	1	1	1	0	0	0	0
8	1	1	1	1	1	1	0	0	1	1	1
…	…										
171	0	0	0	0	0	0	0	1	1	1	0
172	0	0	0	0	0	0	0	0	1	1	1
173	0	0	0	0	0	0	0	0	0	1	1
174	0	0	0	0	0	0	0	0	0	0	1
175	0	0	0	0	0	0	0	0	0	0	0

Future case	Modes during $t+1 \sim t+4$			
	$t+1$	$t+2$	$t+3$	$t+4$
1	1	1	1	1
2	1	1	1	1
3	1	1	1	1
4	1	1	1	1
5	1	1	1	1
6	1	1	1	1

Case 2-1	u by post injection			
	$t+1$	$t+2$	$t+3$	$t+4$
C3H6	638.64	224.48	1003.09	1499.29
CO	3894.86	6510.86	13331.43	15740

Case 2-1	Δu by post injection			
	$t+1$	$t+2$	$t+3$	$t+4$
C3H6	-411.96	-414.16	778.61	496.2
CO	-2976.57	2616	6820.57	2408.57
T	-5.17	8.25	8.25	8.25

Figure 2.1: Application example of the post injection map

2.2 Catalyst model

2.2.1 Diesel oxidation catalyst

Typical diesel oxidation catalyst (DOC) uses a platinium group metal (PGM)-based catalyst coating with monolith honeycomb substrate. The honeycomb structure is composed of identical square channels, and its cross section is drawn in figure 2.2. $\mathbf{CO}$ and $\mathbf{HC}$ should be diffused into the washcoat pore in order to react with $\mathbf{O_2}$ on the metal active site, and relavant mass balance equations of flow-through monolith are described in the table 2.3 [16, 5]. Only global kinetics are considered for simplification, and they are based on the Langmuir-Hinshelwood mechanism as expressed in the table 2.2 [16, 5]. Since oxidation reactions are highly exothermic, energy balance equations must be considered, and they are also described in the table 2.3 [16, 5]. Note that the nomenclature of symbols in governing equations is explained in the table 2.1.

One challenge of solving governing equations is that these are partial differential equations (PDEs), therefore it should be converted to ordinary differential equations (ODEs) to reduce the computational burden. It can be achieved by applying method of line (MOL) by discretizing the z-axis into 4 identical zones, in other words, states are calculated at 5 positions.

Other major role of diesel oxidation catalyst is to elevate the DPF inlet temeperature that is needed for active regeneration by oxidation reactions from additional fuel. For this reason, the main objective function of PM controller should be constructed to track the target DPF inlet temperature [15]. In order to achieve this objective, mathematical models of post injection and DOC are required.

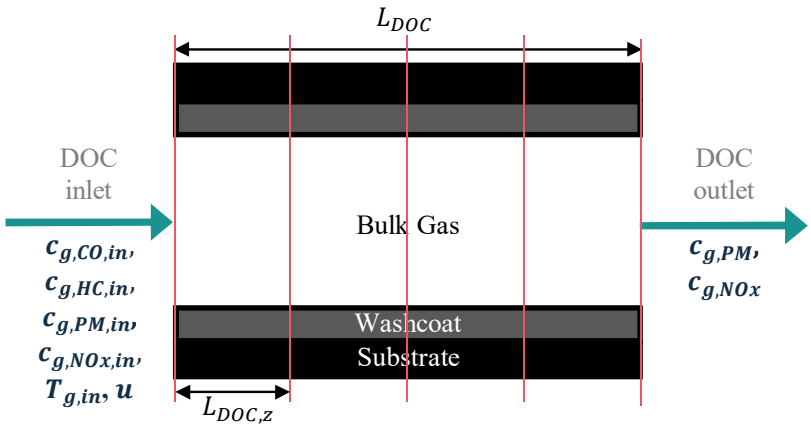

Figure 2.2: Model of diesel oxidation catalyst

Table 2.1: Nomenclature of symbols in governing equations

Nomenclature	
ϕ	volume fraction with respect to reactor volume $[-]$
C	gas concentration $[\mathrm{mol/m^3}]$
T	temperature [K]
ρ	density $[\mathrm{kg/m^3}]$
c_p	heat capacity at constant pressure $[\mathrm{J/kg \cdot K}]$
H_f	enthalpy of formation [J/mol]
u	gas velocity [m/s]
t	time [s]
z	axial position [m]
k_c	coefficient for mass transfer [m/s]
k_h	coefficient for heat transfer $[\mathrm{J/m^2 \cdot K \cdot s}]$
λ	thermal conductivity $[\mathrm{J/m \cdot K \cdot s}]$
a	gas/solid interfacial area to volume ratio $[\mathrm{m^2}/m^3]$
ν	reaction coefficient $[-]$
r	reaction rate $[\mathrm{mol/m^3} \cdot s]$
θ	degree of surface coverage $[-]$
Γ	surface site density of catalyst $[\mathrm{mol/m^3}]$

Subscripts	
i	reaction index
j	species index
m	adsorbed intermediates ($\mathrm{NH_3} - \mathrm{S}$)
g	bulk gas
wc	washcoat pores
s	solid (except washcoat pores)

Table 2.2: Reactions of diesel oxidation catalyst

i	Reactions	Kinetics	Reaction name
1	$CO + 0.5O_2 \rightarrow CO_2$	$r_1 = k_1 x_{CO} x_{O_2} / G_{tot}$	CO oxidation
2	$C_3H_6 + 4.5O_2 \rightarrow 3CO_2 + 3H_2O$	$r_2 = k_2 x_{C_3H_6} x_{O_2} / G_{tot}$	C_3H_6 oxidation
3	$NO + 0.5O_2 \leftrightarrow NO_2$	$r_3 = k_3 x_{NO} x_{O_2} (1 - K'/K_{eq}) / G_{tot}$	NO oxidation

Table 2.3: Governing equations of diesel oxidation catalyst

(1) Concentrations of the gas in the bulk gas layer
$$\frac{\partial C_{g,j}}{\partial t} + u\frac{\partial C_{g,j}}{\partial z} = -\frac{k_{c,j}a}{\phi_g}\left(C_{g,j} - C_{wc,j}\right)$$
(2) Concentrations of the gas in the pores of washcoat layer
$$\frac{\partial C_{wc,j}}{\partial t} = \frac{k_{c,j}a}{\phi_{wc}}\left(C_{g,j} - C_{wc,j}\right) + \sum\nolimits_i \nu_{ji} r_i$$
(3) Temperature of the gas in the bulk gas layer
$$\rho_g c_{p,g}\left(\frac{\partial T_g}{\partial t} + u\frac{\partial T_g}{\partial z}\right) = -\frac{k_h a}{\phi_g}\left(T_g - T_s\right)$$
(4) Temperature of the solid surface
$$\rho_s c_{p,s}\frac{\partial T_s}{\partial t} = \lambda_s\frac{\partial^2 T_s}{\partial z^2} + \frac{k_h a}{\phi_s}\left(T_g - T_s\right) - \frac{\phi_{wc}}{\phi_s}\sum\nolimits_{i,j} H_{f,j}\nu_{ji} r_i$$

2.2.2 Diesel particulate filter

Diesel particulate filter (DPF) also uses a platinium group metal (PGM)-based catalyst to oxidize PM [3], but has a different geometrical structure compared to DOC as we can see from the cross section of unit cell described in the figure 2.3 [17]. The upper layer and the bottom layer are discriminated by a filter and PM is accumulated in the upper layer.

The thickness of accumulated PM differs by the z-axis, and it can be calculated from the soot mass balance in the table 2.5 [13]. Since accumulated PM interrupts the bulk gas flow, pressure drop through the filter and the momentum balance cannot be ignored, and they are also described in the table 2.5 [13]. It is the biggest difference of wall-flow monolith compared to the flow-through monolith. Therefore, the DPF outlet gas concentration and temperature are calculated by 1D+1D model [17].

PM can be oxidized by two mechanisms; passive regeneration by $\mathbf{NO_2}$ at the temperature range of 250°C $\sim$ 400°C, and active regeneration by $\mathbf{O_2}$ at a temperature above 550°C [6]. More detailed reactions are introduced in the table 2.4 [13]. Note that ninth and tenth reactions are not balanced due to unspecified HC. Since active regeneration requires higher temperature, it needs additional fuel. For this reason, maintaining active regeneration mechanism always is inefficient in the perspective of fuel efficiency. Therefore, calculation of PM accumulation is necessary and this is the reason why DPF model is needed. If PM accumulation exceeds the threshold, this information is transmitted to the switching controller, to convert the $\mathbf{NO}_x$ controller into the PM controller.

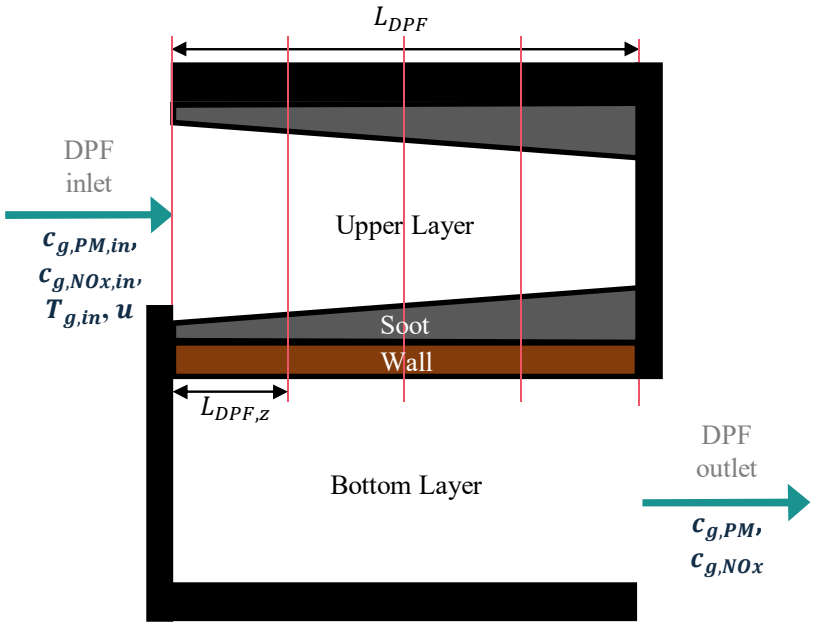

Figure 2.3: Model of diesel particulate filter

Table 2.4: Reactions of diesel particulate filter

i	Reactions	Reaction name
1	$C(s) + O_2 \rightarrow CO_2$	Active regeneration
2	$C(s) + 0.5O_2 \rightarrow CO$	
3	$C(s) + NO_2 \rightarrow CO + NO$	Passive regeneration
4	$C(s) + 2NO_2 \rightarrow CO_2 + 2NO$	
5	$0.5O_2 + N_2 \rightarrow NO$	NO formation
6	$NO + 0.5O_2 \rightarrow NO_2$	NO oxidation
7	$CO + 0.5O_2 \rightarrow CO_2$	CO oxidation
8	$CO + NO_2 \rightarrow CO_2 + NO$	
9*	$HC + O_2 \rightarrow CO_2 + H_2O$	HC oxidation
10*	$HC + NO_2 \rightarrow CO_2 + H_2O + NO$	

Table 2.5: Governing equations of diesel particulate filter

(1) Soot mass balance
$$\frac{\partial m_p}{\partial t} = M^p V_{FVM} \sum_k R_k - E_{DP}$$
(2) Mass balance
$$d_1(z) = d - 2(w(z) + w_{al} + w_{wl}), \qquad d_2 = d$$ $$\frac{\partial(d_1^2 \phi_1)}{\partial z} = -4d\phi_s, \qquad d_2^2 \frac{\partial \phi_2}{\partial z} = 4d\phi_s$$
(3) Component balance
$$\frac{\partial\left(d_i^2 \phi_i y_i^j\right)}{\partial z} = -4d\phi_s y_i^j + 4d_i k_{c,i}^j (y_{s,i}^j - y_i^j)$$
(4) Momentum balance
$$\frac{\partial(d_1^2 p_1)}{\partial z} + \frac{\partial(d_1^2 \phi_1^2/\rho_1)}{\partial z} = -\frac{\alpha\mu\phi_1}{\rho_1}, \qquad \frac{\partial p_2}{\partial z} + \frac{\partial(\phi_2^2/\rho_2)}{\partial z} = -\frac{\alpha\mu\phi_2/\rho_2}{d_2^2}$$
(5) Pressure drop
$$\Delta p_{DPF} = \Delta \mathrm{p}_{\mathrm{contract}} + \Delta p_{inlet} + \Delta p_{soot+ash+washcoat} + \Delta p_{outlet} + \Delta p_{expansion}$$
(6) Enthalpy balance
$$\frac{\partial(d_i^2 C_{p,g} \phi_i T_i)}{\partial z} = 4d_i k_{h,i}(T_s - T_i) - 4d\phi_s c_{p,g} T_i$$
(7) Temperature of the solid surface
$$\frac{\partial T_s}{\partial t} = \frac{\lambda_s}{\rho_s C_{p,s}} \frac{\partial^2 T_s}{\partial z^2} + \frac{S}{A_s \rho_S C_{p,s}} \quad (S = H_{transf} + H_{conv} + H_{react})$$

2.2.3 Urea selective catalytic reduction

Urea selective catalytic reduction is the main part of the diesel exhaust aftertreatment system, and adsorbed ammonia degraded from the injected urea at the high temperature reduces the $\mathbf{NO}_x$ emissions from the diesel engines [3]. Metal-exchanged zeolites like Cu-ZSM-5, Fe-ZSM-5, and Cu-SSZ-13 are typical types of SCR catalyst [18, 3]. However, the geometrical structure of SCR is almost similar to that of DOC as we can see in the figure 2.4, since it is a flow-through monolith [16, 19].

In addition, we can confirm in the table 2.6 that the fastest SCR reaction is processed when there are equimolar ratio of $\mathbf{NO}$ and $\mathbf{NO_2}$ exist [7]. It is actually proved experimentally for metal-exchanged zeolites at the temperature of SCR operation range [20, 21].

For governing equations of SCR expressed in the table 2.7, an equation about the surface coverage of the catalyst is added compared to the governing equations of DOC. This is because the global kinetics in the table 2.6 are based on the Eley-Rideal mechanism [7]. Since the outlet $\mathbf{NO}_x$ and $\mathbf{NH_3}$ concentration are sensitive to the surface coverage, it should be necessarily considered.

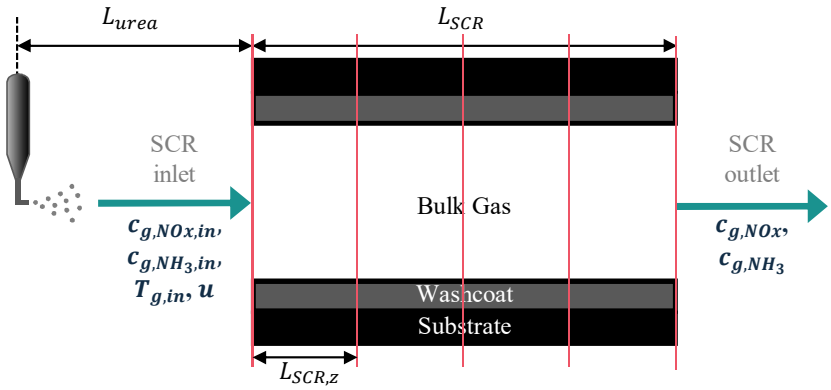

Figure 2.4: Model of urea selective catalytic reduction

Table 2.6: Reactions of urea selective catalytic reduction

i	Reactions	Kinetics	Reaction name
1	$NH_3 + S \rightarrow NH_3 - S$	$r_1 = k_1 C_{NH_3}(1-\theta_m)$	NH_3 adsorption
1r	$NH_3 - S \rightarrow NH_3 + S$	$r_{1r} = k_{1r}\theta_m$	NH_3 desorption
2	$2NH_3 - S + 1.5O_2 \rightarrow N_2 + 3H_2O + 2S$	$r_2 = k_2 C_{O_2}\theta_m$	NH_3 oxidation
3	$NO + 0.5O_2 \leftrightarrow NO_2$	$r_3 = k_3(C_{O_2}^{0.5} C_{NO} - C_{NO_2}/K_3)$	NO oxidation
4	$4NH_3 - S + 4NO + O_2 \rightarrow 4N_2 + 6H_2O + 4S$	$r_4 = k_4 C_{NO}\theta_m$	standard SCR
5	$2NH_3 - S + NO + NO_2 \rightarrow 2N_2 + 3H_2O + 2S$	$r_5 = k_5 C_{NO} C_{NO_2}\theta_m$	fast SCR
6	$4NH_3 - S + 3NO_2 \rightarrow 3.5N_2 + 6H_2O + 4S$	$r_6 = k_6 C_{NO_2}\theta_m$	slow SCR
7	$2NH_3 - S + 2NO_2 \rightarrow N_2 + N_2O + 3H_2O + 2S$	$r_7 = k_7 C_{NO_2}\theta_m$	N_2O formation

Table 2.7: Governing equations of urea selective catalytic reduction

(1) Concentrations of the gas in the bulk gas layer
$$\frac{\partial C_{g,j}}{\partial t} + u\frac{\partial C_{g,j}}{\partial z} = -\frac{k_{c,j}a}{\phi_g}\left(C_{g,j} - C_{wc,j}\right)$$
(2) Concentrations of the gas in the pores of washcoat layer
$$\frac{\partial C_{wc,j}}{\partial t} = \frac{k_{c,j}a}{\phi_{wc}}\left(C_{g,j} - C_{wc,j}\right) + \sum\nolimits_i \nu_{ji} r_i$$
(3) Temperature of the gas in the bulk gas layer
$$\rho_g c_{p,g}\left(\frac{\partial T_g}{\partial t} + u\frac{\partial T_g}{\partial z}\right) = -\frac{k_h a}{\phi_g}\left(T_g - T_s\right)$$
(4) Temperature of the solid surface
$$\rho_s c_{p,s}\frac{\partial T_s}{\partial t} = \lambda_s\frac{\partial^2 T_s}{\partial z^2} + \frac{k_h a}{\phi_s}\left(T_g - T_s\right) - \frac{\phi_{wc}}{\phi_s}\sum\nolimits_{i,j} H_{f,j}\nu_{ji} r_i$$
(5) Surface coverage of the catalyst
$$\frac{\partial \theta_m}{\partial t} = \frac{\sum_i \nu_{m,i} r_i}{\Gamma_m}$$

2.3 Model predictive control with successive linearization method

Due to the highly nonlinear system of diesel engines and diesel exhaust aftertreatment system have and complex constraints of post injection modes, model predictive control is appropriate to find the optimal sequence of post injection modes and urea injection rates. Considering the constraints of post injection modes and sampling time of 1s, prediction horizon and control horizon are fixed to 5s and 4s, respectively, and they are based on a sequence of post injection modes during the last 11s.

The manipulated variable of the post injection controller is a sequence of post injection modes. Since this variable is a discrete variable, using previously created post injection map can reduce the computational load considerably. However, most of the computational time is focused on the integration of ODE catalytic models, so current method that integrates all the possible sequences of post injection modes is still inefficient. In this case, successive linearization method can be a solution. Its mathematical details are introduced in the figure 2.5 [22, 23].

If given ODE models are linearized by successive linearization and the integration results from the previous inputs are calculated already, we can calculate new states by just adding the simple matrix multiplication term to the calculated previous results, without repeated integration. One of the matrix can be easily calculated from the Jacobian matrices of models, and the other matrix is just a state differences that can be easily obtained from the post injection map. If once the state differences of DOC are calculated, they can be applied

to the linearized DPF model, and then to the linearized SCR model, respectively.

The manipulated variable of the urea injection controller is a urea injection rate, which is a continous variable. We can obtain the optimal solution by solving the finite horizon optimal control problem (FHOCP). It will be elucidated in the chapter 3.

$$\begin{bmatrix} x_{k+1} \\ x_{k+2} \\ \cdots \\ x_{k+p} \end{bmatrix} = \begin{bmatrix} F_1(x_k, u_{k-1}) \\ F_2(x_k, u_{k-1}) \\ \cdots \\ F_p(x_k, u_{k-1}) \end{bmatrix} + \begin{bmatrix} B_k & 0 & \cdots & 0 \\ A_k B_k + B_k & B_k & \cdots & 0 \\ \vdots & \vdots & \ddots & \vdots \\ \sum_{i=0}^{p-1} A_k^i B_k & \cdots & \cdots & B_k \end{bmatrix} \begin{bmatrix} \Delta u_k \\ \Delta u_{k+1} \\ \cdots \\ \Delta u_{k+p-1} \end{bmatrix}$$

new states — calculate by ode15s — from Jacobian matrix — from post injection map

Figure 2.5: Application of successive linearization

Chapter 3

Simulation and Results

3.1 Proposed control algorithms

In this thesis, two control algorithms are proposed. Both of them are composed of a post injection controller and an urea injection controller. Post injection controller is composed of a $\mathbf{NO}_x$ controller and a PM controller. The main proposed algorithm is the first one, which uses the fact that the $\mathbf{NO}_x$ reduction performance of SCR is maximized when the $\mathbf{NO2/NO}_x$ ratio is close to $\mathbf{0.5}$. Therefore, the $\mathbf{NO}_x$ controller of the first algorithm is targeted to maintain the $\mathbf{NO2/NO}_x$ ratio at the SCR inlet at the level of $\mathbf{0.5}$.

The second proposed algorithm do not use the optimal $\mathbf{NO2/NO}_x$ ratio that is previously known, instead the $\mathbf{NO}_x$ controller is targeted to reduce the cumulative $\mathbf{NO}_x$ emissions of whole diesel exhaust aftertreatment system. Since it should solve finite horizon optimal control problems (FHOCP) written in the table 3.1 for every possible sequence of post injection modes, second algorithm cannot be used for real-time control. However, it gives the optimal solution to the control problem of whole diesel exhaust aftertreatment system, therefore this solution can be a reference to compare with the first algorithm.

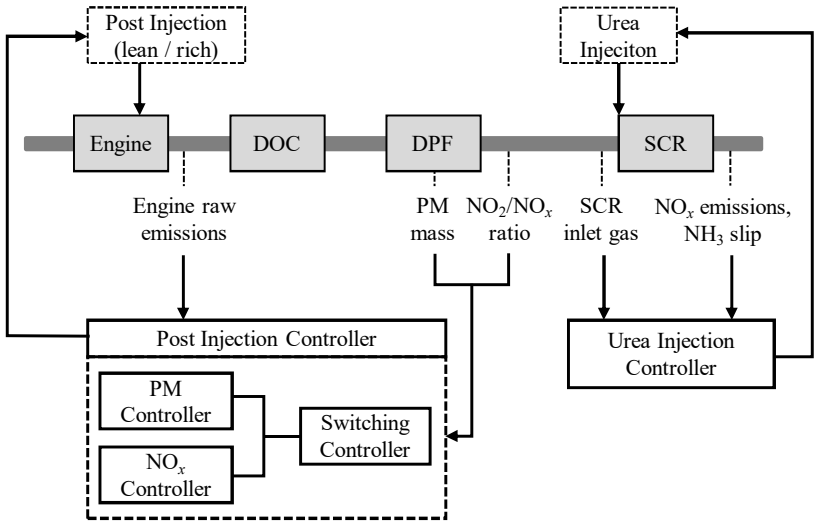

Figure 3.1: Overall control scheme

Table 3.1: Objective functions of two proposed algorithms

Objective functions of algorithm 1		
Post Injection Controller	NOx controller	$\min_{P.I.mode} w_a \frac{N_{rich}}{10} + w_b \sum_{t_k}^{t_k+T_p} \left(\frac{NO_{2,DPFout}(t)}{NO_{x,DPFout}(t)} - 0.5 \right)^2$
	PM controller	$\min_{P.I.mode} \frac{N_{rich}}{10} + \sum_{t_k}^{t_k+T_p} \left(\frac{T_{DPF}(t)}{T_{DPF,target}} - 1 \right)^2$
Urea Injection controlelr		$\min_{\bar{c}_{3,in}} \int_{t_k}^{t_k+T_p} \left(\left\| \frac{\bar{c_1}(s)}{c_{1,in}} \right\|_{Q_1}^{\mathrm{NO}} + \left\| \frac{\bar{c_2}(s)}{c_{2,in}} \right\|_{Q_2}^{\mathrm{NO_2}} + \left\| \frac{\bar{c_3}_{in}(s)}{c_{3,in,max}} \right\|_{R_1}^{\mathrm{NH_3}} \right) ds$

Objective functions of algorithm 2		
Post Injection Controller	NOx controller	$\min_{P.I.mode} \frac{N_{rich}}{10} + \frac{NOx_{cum}}{NOx_{cum,regulation}}$
	PM controller	$\min_{P.I.mode} \frac{N_{rich}}{10} + \sum_{t_k}^{t_k+T_p} \left(\frac{T_{DPF}(t)}{T_{DPF,target}} - 1 \right)^2$
Urea Injection controlelr		$\min_{\bar{c}_{3,in}} \int_{t_k}^{t_k+T_p} \left(\left\| \frac{\bar{c_1}(s)}{c_{1,in}} \right\|_{Q_1}^{\mathrm{NO}} + \left\| \frac{\bar{c_2}(s)}{c_{2,in}} \right\|_{Q_2}^{\mathrm{NO_2}} + \left\| \frac{\bar{c_3}_{in}(s)}{c_{3,in,max}} \right\|_{R_1}^{\mathrm{NH_3}} \right) ds$

3.2 Results and Discussion

Simulation results during 4990s real driving cycle are described in the next 3 pages. Note that the real driving cycle consists of three different cycles; urban, highway, and rural driving.

Figure 3.2 shows the $\mathbf{NO_2}/\mathbf{NO}_x$ tracking performance of proposed two algorithms. For the case of algorithm 1, w_a and w_b are both fixed to 1. Except the highway driving cycle where PM controller is on and $\mathbf{NO}_x$ controller is off, both of two algorithms tract the $\mathbf{0.5}$ ratio. The tracking performance of algorithm 2 is slightly weaker than algorithm 1, because the $\mathbf{NO}_x$ controller of algorithm 2 is not targeted to maintain the $\mathbf{NO_2}/\mathbf{NO}_x$ ratio at the level of $\mathbf{0.5}$. Nevertheless, similar tracking performances of two algorithms implies that the optimal $\mathbf{NO_2}/\mathbf{NO}_x$ ratio at the SCR inlet is nearly $\mathbf{0.5}$.

Furthermore, figure 3.3 shows the cumulative $\mathbf{NO}_x$ emissions of algorithm 1 with $w_a = w_b = 1$ and model predictive control without successive linearization method, compared to the current emission standards. Both of two cases emit less $\mathbf{NO}_x$ compared to the current emission standards, and algorithm 1 shows slightly higher cumulative $\mathbf{NO}_x$ emissions compared to the basic model predictive control algorithm. This is because algorithm 1 has an assumption that the optimal $\mathbf{NO_2}/\mathbf{NO}_x$ at the SCR inlet is $\mathbf{0.5}$. However, algorithm 1 is still more efficient to use for real-time control compared to the basic model predictive control algorithm.

In addition, table 3.2 compares the two proposed algorithms by fuel efficiency, cumulative $\mathbf{NO}_x$ emissions, and cumulative $\mathbf{NH_3}$ injections. Note that all percentage values are relative values compared to the reference case that has no $\mathbf{NO}_x$ controller. Results of cumu-

lative $\mathbf{NO}_x$ emissions and cumulative $\mathbf{NH_3}$ injections show that the algorithm 2 is closer to the optimal solution than algorithm 1, but still requires higher computational load. Algorithm 1 enables users to change the weighting parameters w_a and w_b according to control objectives. Furthermore, both of two parameter settings of algorithm 1 show improved $\mathbf{NO}_x$ reduction efficiency while minimizing the additional fuel.

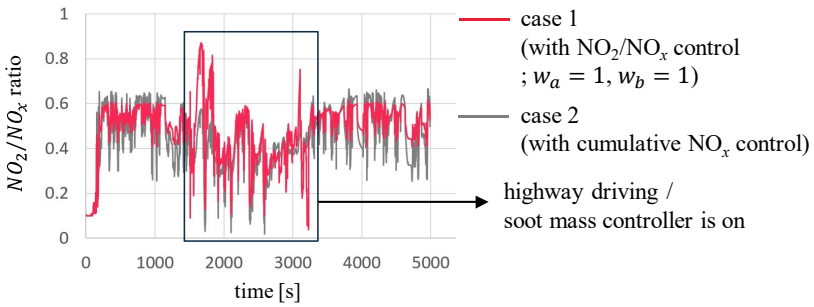

Figure 3.2: $\mathbf{NO_2/NO}_x$ ratio of proposed two algorithms during 4990s driving cycle

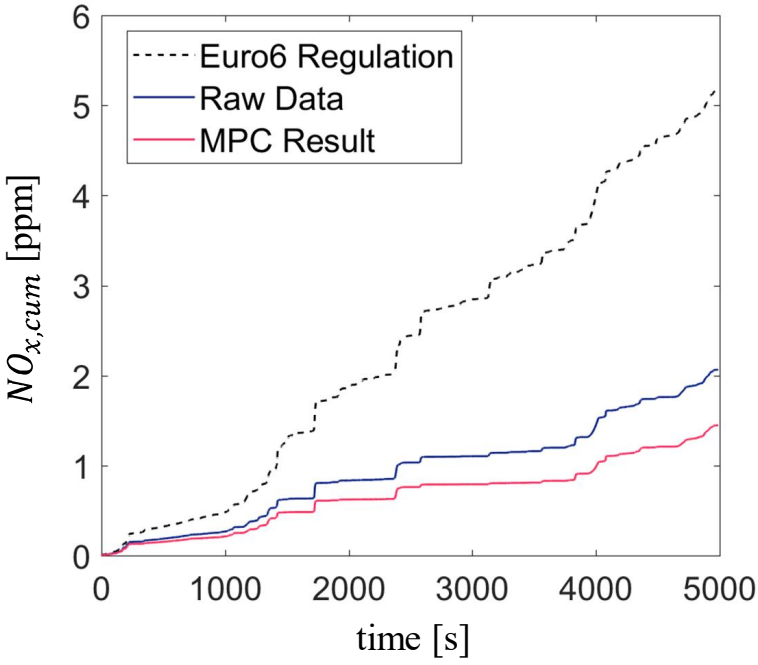

Figure 3.3: Cumulative $\mathbf{NO}_x$ in the SCR outlet

	Algorithm 1		Algorithm 2
	$w_a = 1, w_b = 1$	$w_a = 1.5, w_b = 0.5$	
Number of rich mode	27.1%	22.7%	32.0%
Number of rich mode when soot mass controller is on	-45.7%	-41.7%	-50.0%
Cumulative NO_x emissions	-55.2%	-39.8%	-60.7%
Cumulative NH_3 inlet	-35.9%	-30.1%	-39.2%

Table 3.2: Comparison of proposed two algorithms

Chapter 4

Conclusions

Two model predictive control algorithms of diesel exhaust aftertreatment system are proposed to improve the $\mathbf{NO}_x$ reduction performance of SCR. In order to minimize the computational time, one dimensional catalytic models of DOC, DPF, and SCR are developed, and then post injection map and successive linearization based method are applied. First algorithm uses the fact that the $\mathbf{NO}_x$ removal efficiency of SCR is the maximum when the $\mathbf{NO_2}/\mathbf{NO}_x$ ratio at the SCR inlet is nearly the half, while second algorithm is targeted to reduce the cumulative $\mathbf{NO}_x$ emissions of whole diesel exhaust aftertreatment system. According to the result of the $\mathbf{NO_2}/\mathbf{NO}_x$ ratio, algorithm 1 shows similar $\mathbf{NO}_x$ reduction efficiency compared to the algorithm 2 which has a nearly optimal solution. In addition, the existence of $\mathbf{NO}_x$ controller shows improved $\mathbf{NO}_x$ reduction efficiency while minimizing the amount of additional fuel injections.

These results show the possibility of applying model predictive control for real-driving environments. The problem with computational burden can be solved by introducing succesive linearization based method, and it would contribute to more accurate real-time control using the real data estimated from the attached sensors.

Bibliography

[1] P. Mock and F. Cuenot, "Real-driving emissions test procedure for exhaust gas pollutant emissions of cars and light commercial vehicles in europe," *Int. Counc. Clean Transp*, 2017.

[2] T. Johnson, "Diesel engine emissions and their control," *Platinum Metals Review*, vol. 52, no. 1, pp. 23–37, 2008.

[3] İ. A. Reşitoğlu, K. Altinişik, and A. Keskin, "The pollutant emissions from diesel-engine vehicles and exhaust aftertreatment systems," *Clean Technologies and Environmental Policy*, vol. 17, no. 1, pp. 15–27, 2015.

[4] H. Burtscher, "Physical characterization of particulate emissions from diesel engines: a review," *Journal of Aerosol Science*, vol. 36, no. 7, pp. 896–932, 2005.

[5] T. J. Wang, S. W. Baek, and J.-H. Lee, "Kinetic parameter estimation of a diesel oxidation catalyst under actual vehicle operating conditions," *Industrial & Engineering Chemistry Research*, vol. 47, no. 8, pp. 2528–2537, 2008.

[6] I. P. Kandylas and G. C. Koltsakis, "No2-assisted regeneration of diesel particulate filters: a modeling study," *Industrial & engineering chemistry research*, vol. 41, no. 9, pp. 2115–2123, 2002.

[7] L. Olsson, H. Sjövall, and R. J. Blint, "A kinetic model for ammonia selective catalytic reduction over cu-zsm-5," *Applied Catalysis B: Environmental*, vol. 81, no. 3-4, pp. 203–217, 2008.

[8] E. Cauda, A. Bugarski, and L. Patts, "Diesel aftertreatment control technologies in underground mines: the no2 issue," in *Proceedings of the 13th US/North American Mine Ventilation Symposium*, pp. 17–24, 2010.

[9] T. V. Johnson, "Review of diesel emissions and control," *International Journal of Engine Research*, vol. 10, no. 5, pp. 275–285, 2009.

[10] O. Mihai, C. R. Widyastuti, A. Kumar, J. Li, S. Y. Joshi, K. Kamasamudram, N. W. Currier, A. Yezerets, and L. Olsson, "The effect of no 2/no x feed ratio on the nh 3-scr system over cu–zeolites with varying copper loading," *Catalysis letters*, vol. 144, no. 1, pp. 70–80, 2014.

[11] C. He, J. Li, Z. Ma, J. Tan, and L. Zhao, "High no2/nox emissions downstream of the catalytic diesel particulate filter: An influencing factor study," *Journal of Environmental Sciences*, vol. 35, pp. 55–61, 2015.

[12] D. B. Olsen, M. Kohls, and G. Arney, "Impact of oxidation catalysts on exhaust no2/nox ratio from lean-burn natural gas engines," *Journal of the Air & Waste Management Association*, vol. 60, no. 7, pp. 867–874, 2010.

[13] M. Schejbal, J. Štěpánek, P. Kočí, M. Marek, and M. Kubíček, "Sequence of monolithic converters doc–cdpf–nsrc for lean exhaust gas detoxification: A simulation study," *Chemical Engineering and Processing: Process Intensification*, vol. 49, no. 9, pp. 943–952, 2010.

[14] Y. Kim, T. Park, C. Jung, C. H. Kim, Y. W. Kim, and J. M. Lee, "Hybrid nonlinear model predictive control of lnt and urealess scr aftertreatment system," *IEEE Transactions on Control Systems Technology*, vol. 27, no. 5, pp. 2305–2313, 2018.

[15] O. Lepreux, Y. Creff, and N. Petit, "Model-based temperature control of a diesel oxidation catalyst," *Journal of Process Control*, vol. 22, no. 1, pp. 41–50, 2012.

[16] C. Depcik and D. Assanis, "One-dimensional automotive catalyst modeling," *Progress in energy and combustion science*, vol. 31, no. 4, pp. 308–369, 2005.

[17] E. J. Bissett, "Mathematical model of the thermal regeneration of a wall-flow monolith diesel particulate filter," *Chemical Engineering Science*, vol. 39, no. 7-8, pp. 1233–1244, 1984.

[18] L. Olsson, K. Wijayanti, K. Leistner, A. Kumar, S. Y. Joshi, K. Kamasamudram, N. W. Currier, and A. Yezerets, "A multi-site kinetic model for nh3-scr over cu/ssz-13," *Applied Catalysis B: Environmental*, vol. 174, pp. 212–224, 2015.

[19] C. Depcik, D. Assanis, and K. Bevan, "A one-dimensional lean no x trap model with a global kinetic mechanism that includes nh3 and n2o," *International Journal of Engine Research*, vol. 9, no. 1, pp. 57–77, 2008.

[20] P. S. Metkar, V. Balakotaiah, and M. P. Harold, "Experimental study of mass transfer limitations in fe-and cu-zeolite-based nh3-scr monolithic catalysts," *Chemical engineering science*, vol. 66, no. 21, pp. 5192–5203, 2011.

[21] P. S. Metkar, M. P. Harold, and V. Balakotaiah, "Experimental and kinetic modeling study of nh3-scr of nox on fe-zsm-5, cu-chabazite and combined fe-and cu-zeolite monolithic catalysts," *Chemical engineering science*, vol. 87, pp. 51–66, 2013.

[22] H. SEKI, S. OOYAMA, and M. OGAWA, "Nonlinear model predictive control using successive linearization," *Transactions of the Society of Instrument and Control Engineers*, vol. 38, no. 1, pp. 61–66, 2002.

[23] J. H. Lee and N. L. Ricker, "Extended kalman filter based nonlinear model predictive control," *Industrial & Engineering Chemistry Research*, vol. 33, no. 6, pp. 1530–1541, 1994.

초 록

이 학위논문은 후분사 및 요소수 분사 제어를 이용하여 디젤 배기가스 후처리 시스템의 $\mathbf{NO}_x$ 제거 효율을 극대화할 수 있는 비선형 모델예측제어 기법을 제안한다. 우선 디젤 배기가스 후처리 시스템을 모사하기 위해 디젤 산화촉매 (DOC), 디젤 입자상물질 저감장치 (DPF), 선택적 환원촉매 (SCR)로 구성되는 일련의 촉매 변환기에 대한 1차원 모델을 설계한다. 또한 리치 모드 조작이 엔진 배출가스의 농도와 온도를 어떻게 변화시키는지를 설명하는 후분사맵이 구축되었다. SCR 전단의 $\mathbf{NO_2}/\mathbf{NO}_x$ 비가 0.5일 때 SCR의 $\mathbf{NO}_x$ 제거 효율이 최대가 된다는 사실을 이용하여 $\mathbf{NO}_x$ 제어기와 PM 제어기로 구성된 후분사 제어기를 설계하였다. 추가로, 모델예측제어의 실시간 적용을 위해 계산 비용을 줄이는 방법으로 연속적 선형화 기반의 기법이 사용되었다. 그 결과로 제안된 제어 기법은 $\mathbf{NO}_x$ 제어기가 없는 경우와 비교할 때 추가적인 연료 소모를 최소화하면서 누적 $\mathbf{NO}_x$ 방출량을 절반보다 많이 감소시킴을 확인하였다.

주요어 : 엔진 제어, 모델예측제어, 디젤 산화촉매 (DOC), 디젤 입자상물질 저감장치 (DPF), 선택적 환원촉매 (SCR)
학번 : 2018-23056